

Spreading of Denmark Strait Overflow Water in the Western Subpolar North Atlantic: Insights from Eddy-Resolving Simulations with a Passive Tracer

XIAOBIAO XU

Center for Ocean–Atmospheric Prediction Studies/Florida State University, Tallahassee, Florida

PETER B. RHINES

University of Washington, Seattle, Washington

ERIC P. CHASSIGNET

Center for Ocean–Atmospheric Prediction Studies/Florida State University, Tallahassee, Florida

WILLIAM J. SCHMITZ JR.

Woods Hole Oceanographic Institute, Woods Hole, Massachusetts

(Manuscript received 25 August 2014, in final form 24 February 2015)

ABSTRACT

The oceanic deep circulation is shared between concentrated deep western boundary currents (DWBCs) and broader interior pathways, a process that is sensitive to seafloor topography. This study investigates the spreading and deepening of Denmark Strait overflow water (DSOW) in the western subpolar North Atlantic using two $1/12^\circ$ eddy-resolving Atlantic simulations, including a passive tracer injected into the DSOW. The deepest layers of DSOW transit from a narrow DWBC in the southern Irminger Sea into widespread westward flow across the central Labrador Sea, which reemerges along the Labrador coast. This abyssal circulation, in contrast to the upper levels of overflow water that remain as a boundary current, blankets the deep Labrador Sea with DSOW. Farther downstream after being steered around the abrupt topography of Orphan Knoll, DSOW again leaves the boundary, forming cyclonic recirculation cells in the deep Newfoundland basin. The deep recirculation, mostly driven by the meandering pathway of the upper North Atlantic Current, leads to accumulation of tracer offshore of Orphan Knoll, precisely where a local maximum of chlorofluorocarbon (CFC) inventory is observed. At Flemish Cap, eddy fluxes carry $\sim 20\%$ of the tracer transport from the boundary current into the interior. Potential vorticity is conserved as the flow of DSOW broadens at the transition from steep to less steep continental rise into the Labrador Sea, while around the abrupt topography of Orphan Knoll, potential vorticity is not conserved and the DSOW deepens significantly.

1. Introduction

The deep circulation of the Atlantic Ocean involves concentrated deep western boundary currents (DWBCs), yet it has long been apparent from tracer observations that the deepest flows also spread widely across deep basins (e.g., LeBel et al. 2008). This occurs in the subpolar Labrador Sea and Iceland basin and in the Newfoundland basin. Farther south, eddy-driven recirculations force

deep boundary currents offshore (e.g., Bower et al. 2009, 2011) and are prominent in eddy-resolving models (e.g., Holland and Rhines 1980).

Overflow through the Denmark Strait provides a key pathway for the dense water formed in the Nordic Seas to enter the deep North Atlantic Ocean (e.g., Ross 1984; Girtton and Sanford 2003; Jochumsen et al. 2012). After flowing over the sill (~ 620 m) and entraining ambient water, the Denmark Strait overflow water (DSOW) forms the deepest component of North Atlantic Deep Water (NADW), which also includes the overlying Iceland–Scotland overflow water (ISOW) and Labrador Sea Water (LSW). NADW flows southward as the lower

Corresponding author address: X. Xu, COAPS/Florida State University, 2000 Levy Avenue, Building A, Tallahassee, FL 32306.
E-mail: xxu@coaps.fsu.edu

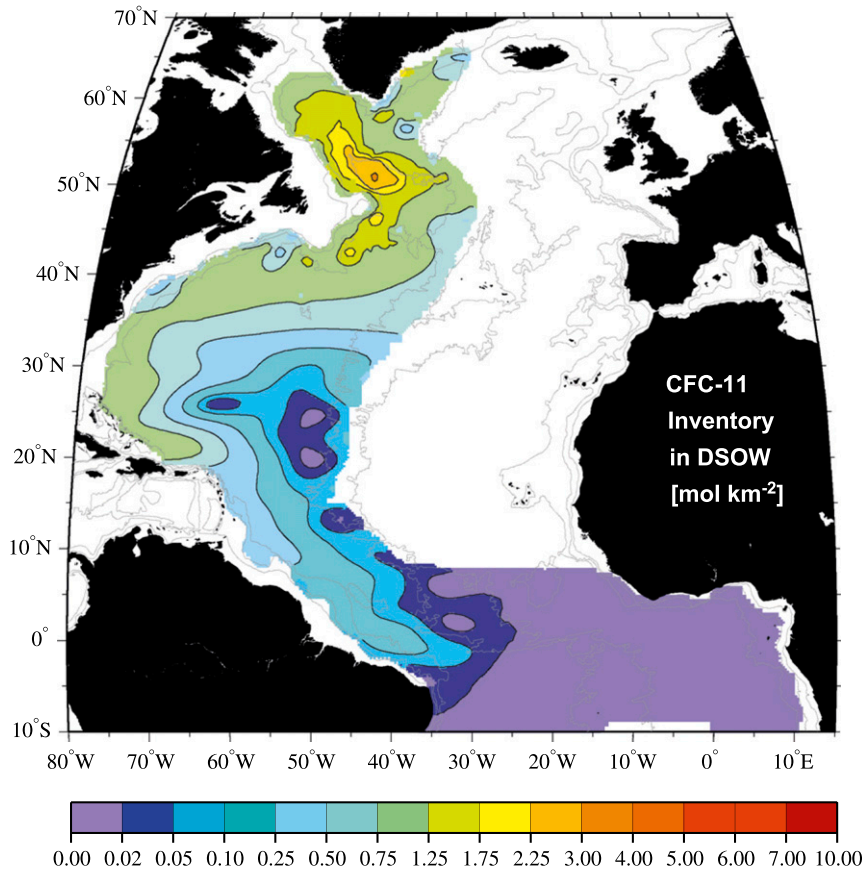


FIG. 1. Observed distribution of CFC-11 inventories (mol km^{-2}) in the DSOW from [LeBel et al. \(2008, their Fig. 9\)](#).

limb of the Atlantic meridional overturning circulation (AMOC) and plays an important role in redistributing heat and freshwater in Earth's climate system.

The large-scale flow pattern of the DSOW (and other components of NADW) in the North Atlantic can easily be extracted from maps of potential temperature θ and salinity S (e.g., [Worthington and Wright 1970](#)). The reader is also referred to [Dickson et al. \(2002\)](#), [Yashayaev \(2007\)](#), and [Yashayaev and Dickson \(2008\)](#) for an extensive data-based discussion on the long-term hydrographic change associated with the DSOW and other NADW components and the transformation of these deep water masses as they spread in the subpolar North Atlantic due to diapycnal and isopycnal mixings. Consistent flow patterns of the DSOW are also derived from tracers such as the chlorofluorocarbons (CFCs; e.g., [Smethie et al. 2000](#); [Smethie and Fine 2001](#); [LeBel et al. 2008](#)), oxygen ([Pickart et al. 2002](#)), tritium ([Jenkins and Rhines 1980](#)), and iodine-129 (^{129}I ; [Smith et al. 2005](#)), and so on. High tracer concentrations associated with the cold and relatively fresh DSOW are found in the DWBCs, in general agreement with the high velocity

cores observed along the western boundary in the subpolar North Atlantic (e.g., [Dickson and Brown 1994](#); [Dickson et al. 2008](#); [Bacon and Saunders 2010](#); [Fischer et al. 2004, 2010](#); [Clarke et al. 1998](#); [Schott et al. 2004, 2006](#)) and in the subtropical regions (e.g., [Toole et al. 2011](#); [Bryden et al. 2005](#); [Johns et al. 2008](#)).

Elevated tracer concentrations and inventories are observed several hundred kilometers away from the DWBC as well. In the Labrador Sea, [Smith et al. \(2005\)](#) show that the DSOW, characterized by high ^{129}I and CFC concentrations, “paints” the entire deepest part of the basin (~ 600 km wide). Extensive hydrographic sections perpendicular to the AR7W line in [Smith et al. \(2005\)](#) also show the presence of DSOW through high dissolved oxygen, CFC, and salinity anomaly, verifying the extent of the “blanket” throughout the deep Labrador Sea. Farther south, the observed CFC inventories (defined as the amount of CFC tracer per unit area) for the DSOW exhibit a clear local maximum in the area offshore of Orphan Knoll (OK) and Flemish Cap (see [Fig. 1](#)). These results led us to focus our attention on how the DSOW and the associated tracer spread from the fast-flowing

DWBC into the deep interior, which is the central question to be examined in this study.

Several studies in recent years have investigated the export of the upper NADW using RAFOS floats and numerical particles (Bower et al. 2009, 2011; Gary et al. 2011). These studies demonstrate the importance of the interior pathways in exporting LSW into the subtropical North Atlantic. Lozier et al. (2013) performed a similar analysis for overflow water using numerical particles launched within the DWBC at 53°N, based on the $1/12^\circ$ Family of Linked Atlantic Modeling Experiments (FLAME; Böning et al. 2006; Biastoch et al. 2008). The probability density of particle positions showed that the overflow water, similar to LSW, is not restricted to the DWBC in its equatorward export. The probability map, as noted, compares favorably with the corresponding maps of CFC inventory in LeBel et al. (2008). However, it is not immediately clear how the probability map of Lagrangian particle positions relates to the volume transport and tracer transport.

In contrast to these studies of the upper NADW, this paper focuses on the circulation of DSOW, the deepest NADW component in the western subpolar North Atlantic. We analyze the circulation primarily in an Eulerian framework, using numerical results from eddy-resolving simulations, including passive tracer injections in DSOW to the north of the Denmark Strait sill. The modeled tracer distribution is shown qualitatively consistent with the observed CFC and ^{129}I distributions associated with the DSOW. We find the following:

- (i) The lowest layers of the DSOW transit from a relatively narrow DBWC in the southern Irminger Sea into widespread westward flow in the central Labrador Sea and regroup along the Labrador coast. This abyssal circulation, in contrast to the upper levels of the overflow water that remain as a relatively narrow boundary current, blankets the deep Labrador Sea with DSOW.
- (ii) Farther downstream, after being steered around the abrupt topography of Orphan Knoll, the DSOW leaves the boundary again, forming recirculation cells in the deep Newfoundland basin. This recirculation beneath the meandering of the North Atlantic Current leads to accumulation of tracer inventory offshore of Orphan Knoll, precisely where a local maximum of CFC inventory is observed.
- (iii) Around the Flemish Cap, eddy flux carries ~20% of the tracer transport of the boundary current offshore and into the interior, contributing to the elevated tracer concentration away from the DWBC.

The rest of the paper is organized as follows: The model configurations are summarized in section 2. In section 3,

we discuss the key model results, focusing on the spreading of the DSOW and its tracer in the Labrador Sea and farther downstream in the Newfoundland basin. A summary and discussion of the findings follows in section 4.

2. Model configurations

Results from eddy-resolving, $1/12^\circ$ Atlantic simulations with the Hybrid Coordinate Ocean Model (HYCOM; Bleck 2002; Chassignet et al. 2003) have been used previously in examining the currents and transports connected with the AMOC (Xu et al. 2010, 2012, 2013, 2014). Particularly relevant to the topic here, Xu et al. (2010) considered the volume transport and θ/S properties of overflow waters after they flow over the Greenland–Scotland Ridge into and within the Irminger Sea. The multiple ISOW pathways in the model [see Kanzow and Zenk (2014) for observational support] provide a possible explanation for the small westward transport observed in ISOW through the Charlie–Gibbs Fracture Zone (CGFZ), which is roughly 60% of deep transport upstream and downstream. Comparison with available long-term moored instrument databases shows reasonable agreement with the observed transports of overflow water with approximately correct θ/S characteristics.

As in Xu et al. (2010), the model domain extends meridionally from 28°S to the Fram Strait at 80°N. No inflow/outflow is prescribed at the northern and southern boundaries. Within a buffer zone of about 3° from these two boundaries, the model θ and S are restored to a monthly ocean climatology, the Generalized Digital Environmental Model (GDEM; Carnes 2009), with an e -folding time of 5–60 days that increases with distance from the boundary. The model was integrated with monthly climatological forcing from the 40-yr European Center for Medium-Range Weather Forecasts (ECMWF) Re-Analysis (ERA-40; Uppala et al. 2005). To better simulate the surface mixed layer, submonthly wind anomalies from the Fleet Numerical Meteorology and Oceanography Center, 3-hourly, 0.5° Navy Operational Global Atmospheric Prediction System (NOGAPS; Rosmond et al. 2002) for the year 2003 were added to the interpolated monthly means.

Building upon Xu et al. (2010), the Atlantic simulations discussed here used vertical resolutions of 32 (model E32) and 64 (model E64) layers, respectively. The reference densities connected with the Nordic Seas overflow water in each experiment are listed in Table 1. A passive tracer was injected into the DSOW in both simulations in order to study the spreading of this water mass. The tracer concentration C was set to 1 kg m^{-3} below 400 m in a rectangular source box upstream of the

TABLE 1. The reference density (σ_2 ; kg m^{-3}) for the model layers that are connected with the Nordic Seas overflow water (NSOW) in the 32- and 64-layer configuration.

E32		E64	
Layer	σ_2	Layer	σ_2
25	36.970	50	36.970
		51	36.995
26	37.020	52	37.020
		53	37.040
27	37.060	54	37.060
		55	37.075
28	37.090	56	37.090
		57	37.100
29	37.110	58	37.110
		59	37.120
30	37.130	60	37.130
		61	37.140
31	37.150	62	37.150
		63	37.175
32	37.200	64	37.200

Denmark Strait sill (Fig. 2a) and 0 everywhere else. To keep a relatively stable tracer flux into the North Atlantic during the model integration, the tracer concentration in the source box was restored toward its initial value, with an e -folding time of 1–10 days increasing from the center toward boundaries of the source box.

Both simulations were integrated for 20 yr. Figure 2b shows the southward tracer flux F into the North Atlantic for the last 5 yr of model simulation. F is an integration of vC , in which v is the meridional velocity, over the full water column and a zonal section across the whole basin. The 5-yr mean tracer flux is $1.68 \times 10^6 \text{ kg s}^{-1}$ in E64 and

$1.65 \times 10^6 \text{ kg s}^{-1}$ in E32. In addition to the time-mean values, the temporal variability of the flux is also similar between the two simulations. The tracer flux exhibits a seasonal cycle associated with the volume transport variability of the DSOW. The DSOW transports in both simulations (not shown) have a mean value of about 3.6 Sverdrups (Sv; $1 \text{ Sv} \equiv 10^6 \text{ m}^3 \text{ s}^{-1}$) and a seasonal variation of about 1 Sv (for monthly mean transports). The results are similar to the estimates of Jochumsen et al. (2012) based on moored ADCP data, in terms of the annual-mean value (3.5 Sv) and the phase of the seasonal variation (high transports in October–November and low transports in May–July), but with a higher magnitude of the variation (by a factor of 2). Part of the seasonal variation in the model is due to overflow contribution over the western shelf, which is outside of the mooring observations.

Although the tracer was injected into the overflow water, some tracer (26% in E64 and 29% in E32; Fig. 2c) escaped the overflow water and entered the layers above the (σ_θ) 27.80 isopycnal due to diapycnal mixing, based on the Richardson number–based K-profile parameterization (KPP; Large et al. 1994) used in HYCOM. The difference in Fig. 2c implies that the diapycnal mixing is slightly weaker in E64 with higher vertical resolution. This can be seen more clearly later in the vertical distribution of the tracer concentration.

3. Key results

In this section, we first present the general picture of the numerical tracer in the North Atlantic, in both horizontal and vertical views (section 3a) and then

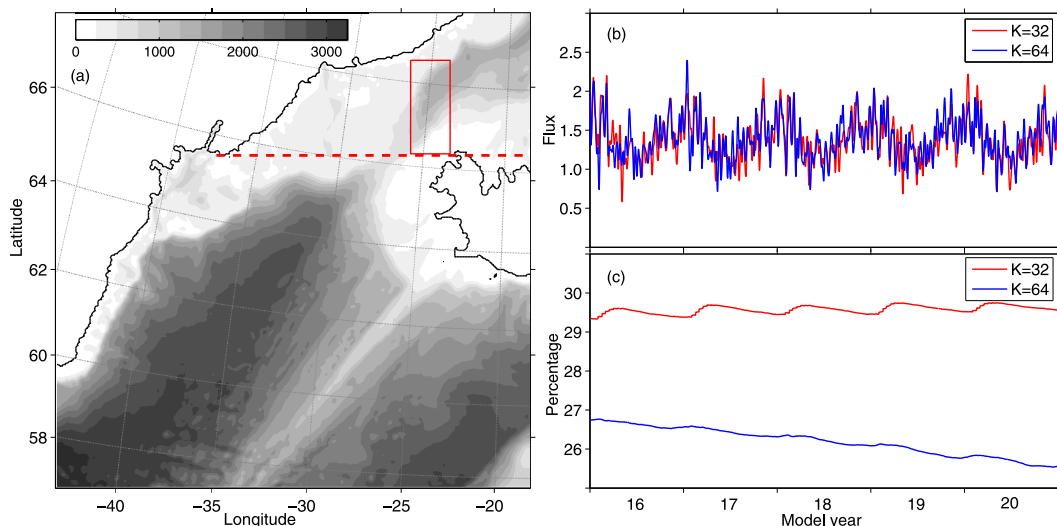


FIG. 2. (a) Model bathymetry around the Denmark Strait. The red box denotes the area where the tracer is injected in model; (b) tracer flux F into the North Atlantic across a zonal section south of the source box, denoted as a red dashed line in (a); (c) percentage of the model tracer inventories that enter the ambient water above (σ_θ) 27.80 kg m^{-3}) due to diapycnal mixing.

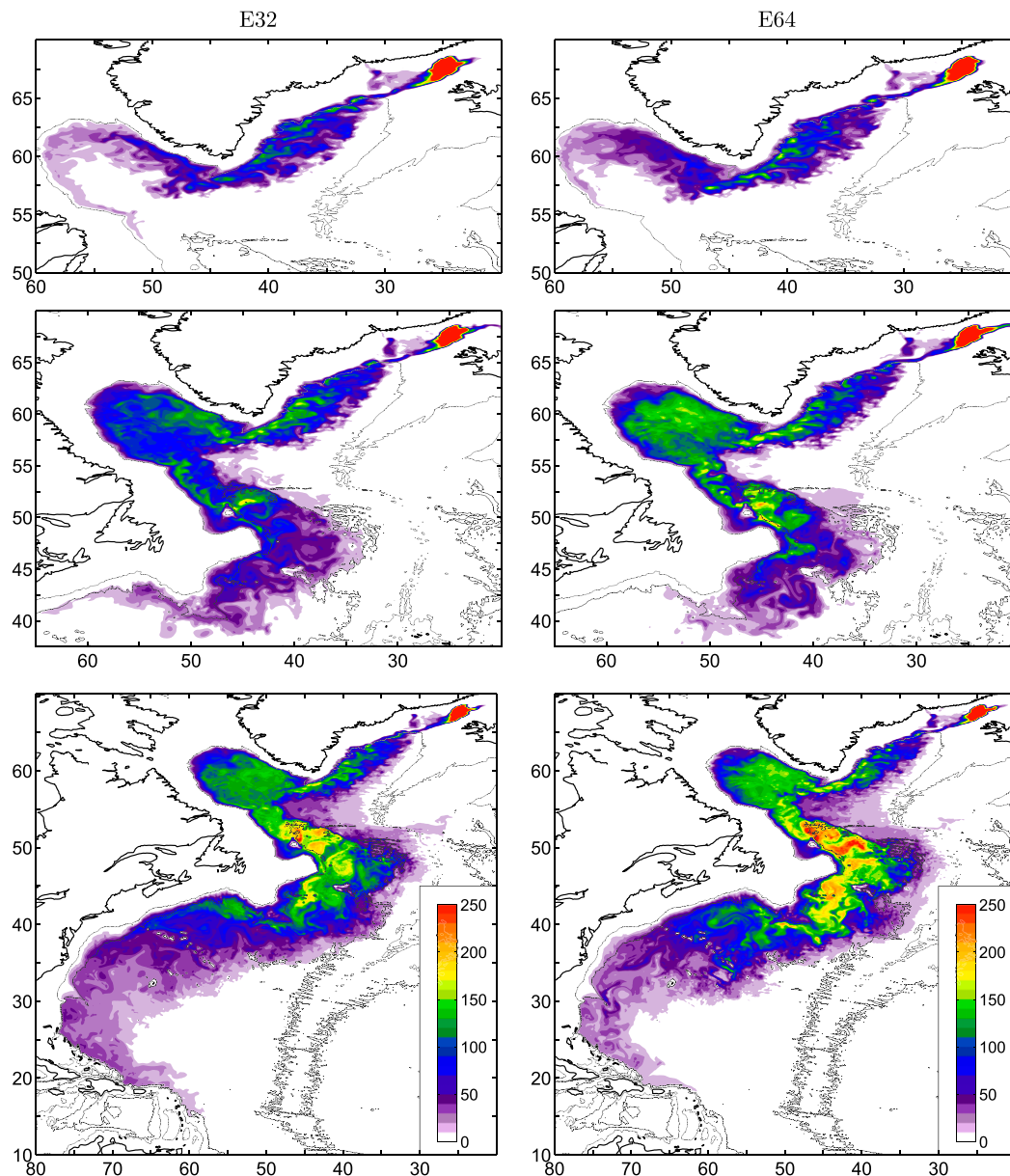


FIG. 3. Snapshot of tracer inventories (kg m^{-2}) below σ_θ of 27.80 kg m^{-3} after (top) 1, (middle) 5, and (bottom) 15 yr of integration in E32 and E64.

examine in more detail the DSOW circulation in the Labrador Sea (section 3b) and farther downstream in the Newfoundland basin (section 3c).

a. General picture of the southward spreading of the DSOW tracer

Snapshots of the modeled tracer inventory (or vertical integration of tracer concentration C) in the overflow water are displayed in Fig. 3. The overflow water is defined as water of density $\sigma_\theta \geq 27.80 \text{ kg m}^{-3}$, a widely used definition in observations. South of the Denmark Strait,

the model DSOW tracer follows the fast-flowing DWBC and the rapidity of this spreading is striking: It takes less than 1 yr for the DSOW to flow around Cape Farewell, Greenland, into the Labrador Sea and about 5 yr to pass the Grand Banks into the western North Atlantic. After 15 yr, the DSOW tracer is visible in the DWBC near 20°N . Jenkins and Rhines (1980) estimated a transition time of 15 yr or less for the DSOW tracer (tritium) to reach the Blake–Bahama Outer Ridge near 30°N , with a dilution factor of 5 to 10. The transition time for the passive tracer in our model is comparable.

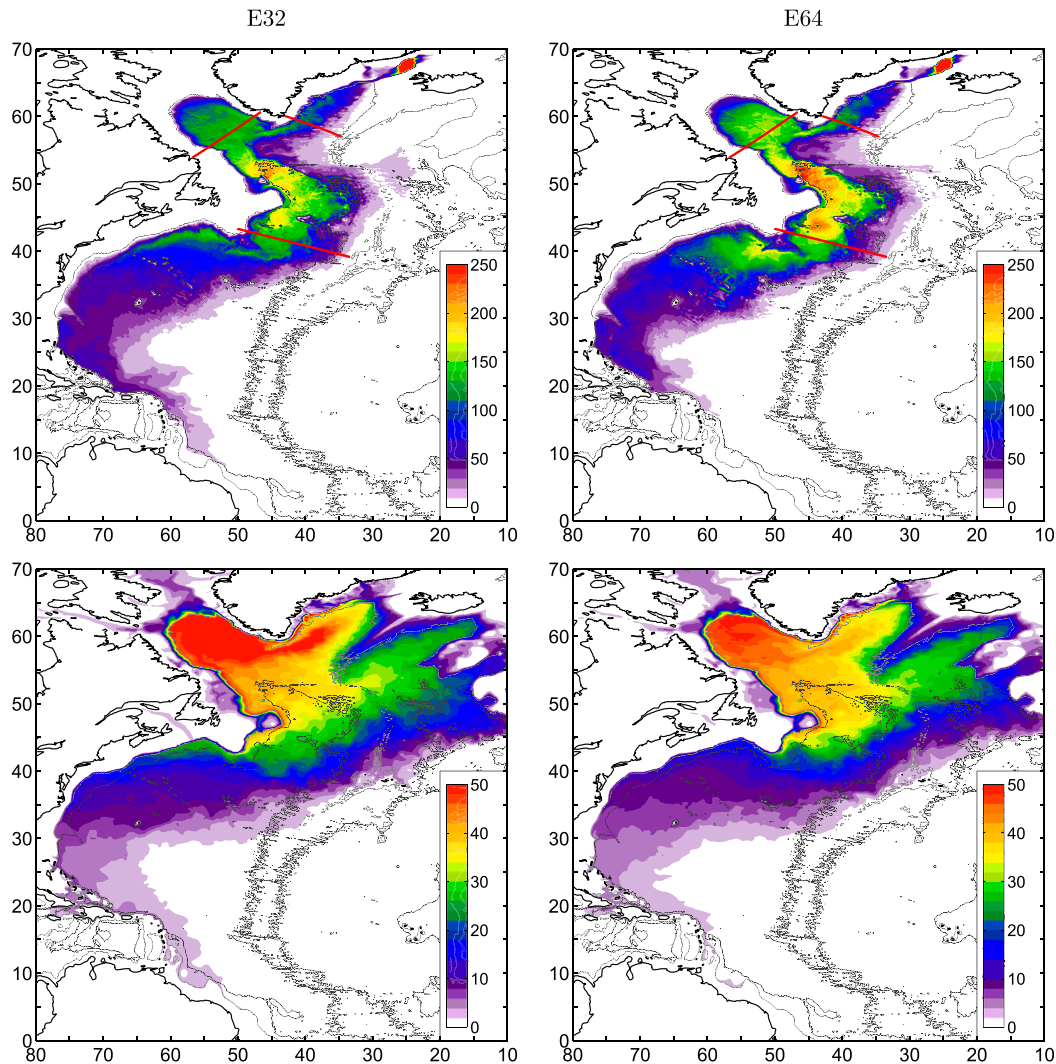


FIG. 4. Horizontal distribution of the annual-mean tracer inventories (kg m^{-2}) based on year 20 in simulations E32 and E64. (top) Inventories for $\sigma_{\theta} \geq 27.80 \text{ kg m}^{-3}$. (bottom) Inventories for $\sigma_{\theta} < 27.80 \text{ kg m}^{-3}$. Note the difference in color scales between the lower and upper layers. The red line in the Labrador Sea denotes a model section, along which the vertical distribution of salinity/tracer is examined in Fig. 5.

The distributions of the annual-mean tracer inventories for model year 20 are displayed in Fig. 4. The model tracer inventories for overflow water qualitatively are strikingly similar to the observed CFC inventories shown in Fig. 1. The latter, from LeBel et al. (2008), represents the input of DSOW into the North Atlantic over the CFC transient time scale of about 3 decades. In both the observations and model, the tracer inventories are nearly homogenous from the Irminger Sea to the Labrador Sea, and, as observed, DSOW is seen spreading across the entire Labrador Sea basin. A strong, local maximum of tracer inventory is also found in the southern Labrador Sea between Orphan Knoll and Flemish Cap. This area, generally including the whole western

Newfoundland basin, marks an important transition region between the subpolar and subtropical gyres (Rossby 1996). The DWBC passes near and beneath the northward-flowing North Atlantic Current (NAC) in the first of several close encounters between deep and shallow limbs of the AMOC. Farther downstream to the west of the Grand Banks, the high inventory signature extends west and southward along the continental margin of the northwestern Atlantic. Offshore, a higher tracer inventory is found in E64 than in E32.

The tracer inventory in layers above the overflow water is mostly in the LSW, and the distribution (see Fig. 4) bears similarities to the extensive subpolar recirculation observed in spreading pathways of the LSW

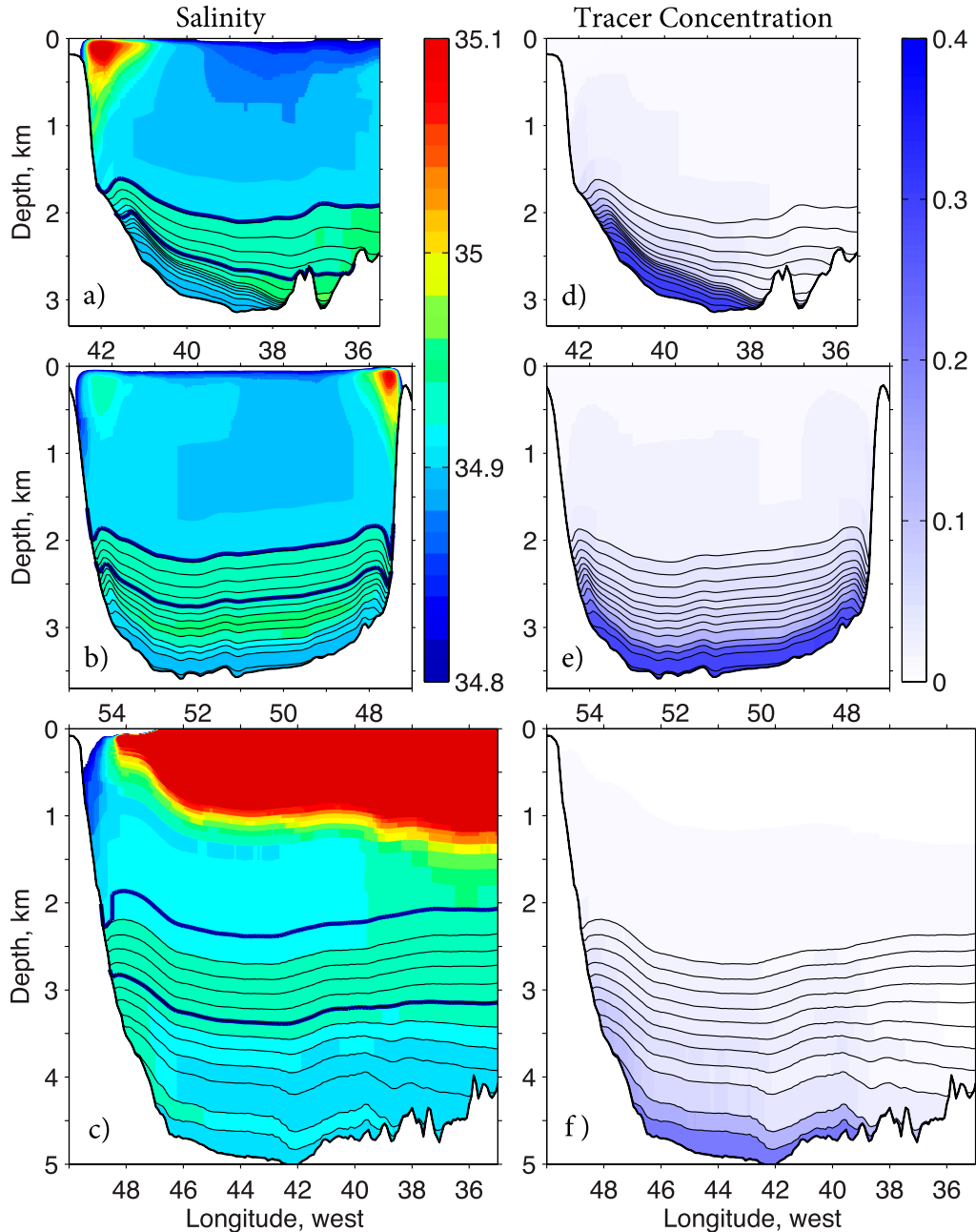


FIG. 5. Annual-mean salinity and tracer concentration along red lines in Fig. 4: (a),(d) southern Irminger Sea; (b),(e) central Labrador Sea; and (c),(f) southern Newfoundland basin. Results based on year 20 in simulation E64. Thin black lines are layer interfaces for overflow water ($\sigma_2 \geq 36.97 \text{ kg m}^{-3}$; Table 1). The two thick blue lines in the left panels are σ_θ of 27.80 and 27.88 kg m^{-3} , respectively.

(e.g., Rhein et al. 2002; Yashayaev et al. 2007): north-eastward into the Irminger Sea, eastward toward the Iceland basin and the Rockall trough, and equatorward into the subtropical North Atlantic.

Figure 5 shows the vertical distributions of the model (E64) salinity and tracer concentration along three sections in the western subpolar North Atlantic:

southeast of the Cape Farewell, Greenland (e.g., Bacon and Saunders 2010); the WOCE/CLIVAR section AR7W in the Labrador Sea (e.g., Lazier et al. 2002; Yashayaev 2007); and southeast of Grand Banks near 43°N (e.g., Schott et al. 2004). These are among the most heavily observed sites in the area and the vertical stacking of the modified North Atlantic Water, LSW,

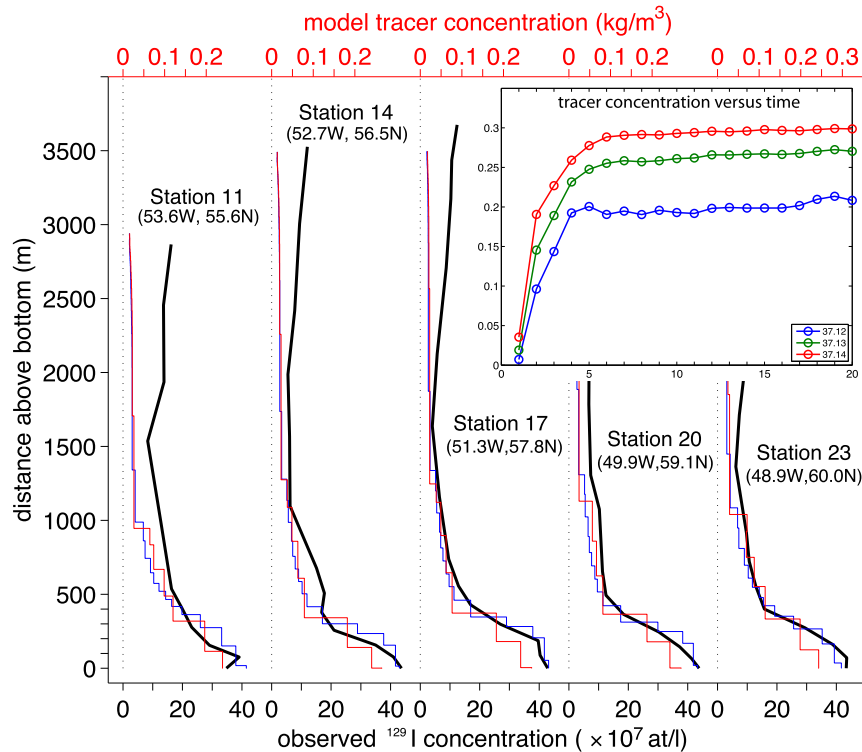


FIG. 6. Vertical profiles of the tracer concentration C at five stations in the Labrador Sea: black lines are the observed ^{129}I from Smith et al. (2005), and colored lines are the last 5-yr means from simulations E32 (red) and E64 (blue). The inset panel shows the time series of C around station 17 for the lowest three layers.

ISOW, and DSOW from top to bottom has been well-documented observationally. The model distributions (similar between E64 and E32) are generally consistent with these observations.

The results in Fig. 5 demonstrate that the modeled DSOW, initially at 400–620 m at the Denmark Strait sill, spreads across the entire 600-km-wide deep Labrador Sea below 2500 m. Many hydrographic sections in the region have shown anomalously high oxygen, CFCs, tritium, and other classic tracers in this abyssal layer. Radioactive tracers, injected into surface waters from nuclear reprocessing plants at Sellafield (United Kingdom) and La Hague (France), provide particularly vivid images of circulation into the Nordic Seas and returning south to the Atlantic in the dense overflows (Smith et al. 2005). The ^{129}I released in the early 1990s appeared in the Denmark Strait 5 to 7 yr later. Its pathway, from the source through the Nordic Seas and into the Atlantic, has been modeled at $1/2^\circ$ lateral resolution by Orre et al. (2009), in remarkably rapid transit through a sequence of boundary currents, basin flows, and overflows. This supports the “fast-track” conversion of warm northward-flowing AMOC waters to dense northern overflow waters (Mauritzen 1996).

Our numerical tracer experiments are designed to investigate modeled pathways and transitions within the western subpolar North Atlantic. In Fig. 6, the time-mean (years 16–20) vertical profile of the numerical tracer at five locations along the AR7W section is compared to that of observed ^{129}I (Smith et al. 2005). Both the observation- and model-based profiles show a clear increase of tracer concentration toward the bottom in the lowest ~ 400 m above the seafloor. This suggests that the vertical structure of the modeled DSOW tracer in this area is consistent with the observations (the discrepancy in the upper ocean is due in part to the model tracer entering the North Atlantic through overflow water only, whereas ^{129}I enters through surface layers as well). Considering the time series of the model tracer in the central Labrador Sea (inset panel in Fig. 6), the major increase of tracer concentration takes 3–4 yr and a relatively stable state is reached about 6 yr after injection begins near the Denmark Strait. In comparison, the buildup of ^{129}I in the central Labrador Sea takes a minimum of 6 yr from the time it passes through the strait in 1995 (Smith et al. 2005, their Fig. 2). A modest bottom intensification of the tracer concentration is observed in the central Labrador Sea in 1997, followed

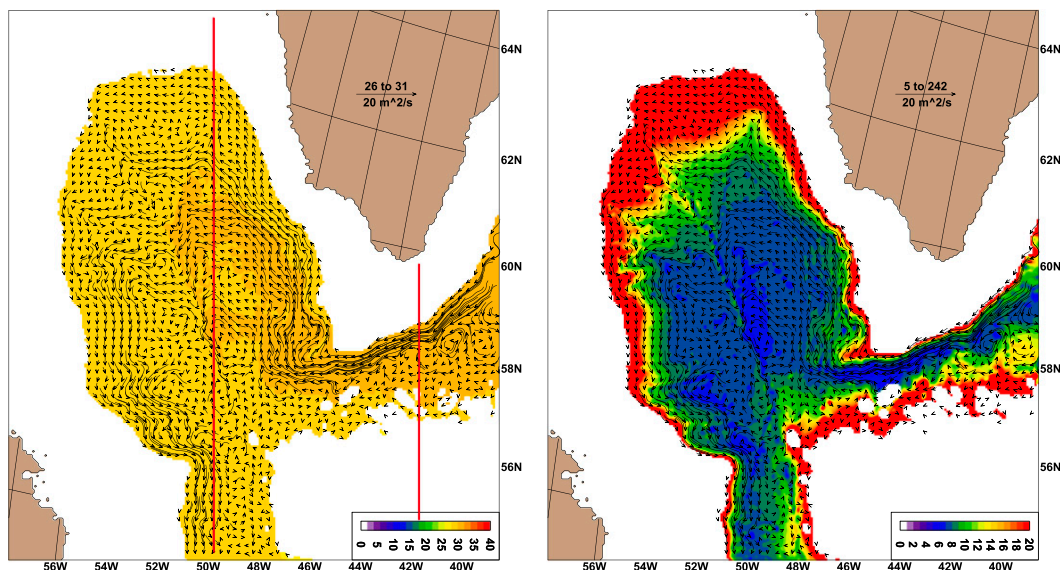


FIG. 7. Vector of the volume transport per unit width ($\text{m}^2 \text{s}^{-1}$) on the distributions of (left) tracer concentration ($10^{-2} \text{ kg m}^{-3}$) and (right) potential vorticity ($10^{-7} \text{ m}^{-1} \text{ s}^{-1}$) for the lower overflow water ($\sigma_2 \geq 37.14 \text{ kg m}^{-3}$) based on a 5-yr mean of simulation E64 (years 16–20).

by a 300% increase in tracer concentration during 1997–2001. The more rapid buildup of the model tracer is likely due to its sudden injection at the strait, compared to the gradual increase of ^{129}I following its long path (to the strait).

The model DSOW tracer also occupies the deepest portion of the Newfoundland basin southeast of Grand Banks near 43°N (Fig. 5f), whereas the DSOW signature at this location is more along the western boundary in observations (Clarke et al. 1980). A deeper/denser DSOW in model, compared with observations, becomes clearer farther downstream in the subtropical North Atlantic, indicating that the diapycnal mixing in the model is somewhat weaker than observed.

b. The spreading of DSOW in the Labrador Sea

Figures 4–6 show that the model DSOW tracer, similar to observations of Smith et al. (2005) and LeBel et al. (2008), spreads across the entire base of the Labrador Sea. This is especially clear for the bottom two layers in Fig. 5d ($\sigma_2 \geq 37.14 \text{ kg m}^{-3}$). In Fig. 7a, the time mean, vertically averaged tracer concentration for this lower part of the DSOW is overlaid with vectors of the mean transport per unit width. Abyssal DSOW is seen to transit from a narrow boundary current southeast of Cape Farewell into widely spread westward flows in the northern and central Labrador Sea. Sensitivity to topography is evident: some of the model westward flows turn southeastward along the small Northwest Atlantic Mid-Ocean Channel (NAMOC), one of the longest deep-sea channels of the world's ocean (Klaucke and

Hesse 1996). The southeast flow in the NAMOC has been observed recently in repeated lowered acoustic Doppler current profiler (LADCP) data in the Labrador Sea (Hall et al. 2013). Figure 7a shows that the water originates from the DWBC to the northeast of Cape Farewell.

In Fig. 7b, the same transport vectors are overlaid on the distribution of potential vorticity (PV), $(f + \zeta)/h$, where f is the Coriolis parameter, ζ is vertical relative vorticity, and h is layer thickness. The dynamical tracer PV in this case illustrates the circulation pattern with low values of PV corresponding to weak stratification of DSOW, compared with the surrounding ocean. The DSOW flows southwestward within the narrow DWBC along the western continental slope of the Irminger Sea. After flowing around the Eirik Ridge into the Labrador Sea, the low PV plume turns westward, flows across the basin, and connects to the DWBC on the western side of the Labrador Sea. The signature of the NAMOC, only a few tens of meters deep in the model bathymetry, is clearly visible in PV (Fig. 7b). Since the DSOW layer is thin, it is very sensitive to small changes in topographic features.

This pattern of near-bottom circulation contrasts significantly with that of the upper overflow water. Figure 8 shows transport vectors on distributions of the tracer concentration C and PV for an upper overflow water of $36.97 \leq \sigma_2 < 37.06 \text{ kg m}^{-3}$. In the upper layer, the overflow water flows around the boundary of the Labrador Sea as a relatively continuous and narrow DWBC (also note the very similar pattern between the passive and dynamical PV tracer).

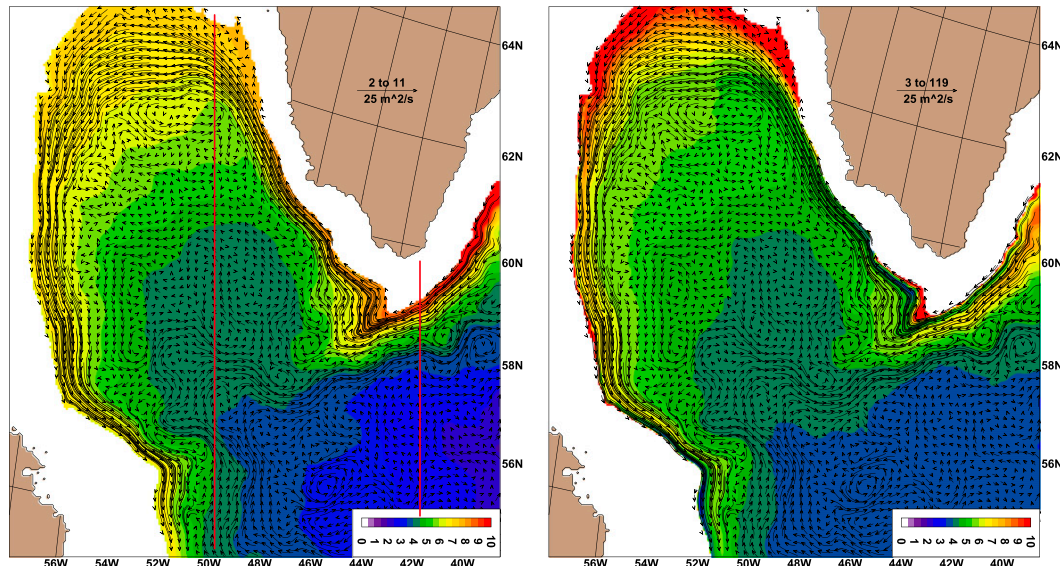


FIG. 8. As in Fig. 7, but for the upper overflow water with $37.97 < \sigma_2 \leq 37.02 \text{ kg m}^{-3}$.

To quantify the relative importance of the DWBC versus the interior flow in carrying the DSOw and its tracer, we calculated the westward fluxes for overflow water across a model section denoted as the red line in the Labrador Sea in Figs. 7–8. The results are shown layer by layer in Fig. 9 for both simulations. In E64, there is a striking difference between the widely spread, weak interior flows in the deep layers (red lines) and the narrow, strong boundary current in the upper layers (blue lines). For all overflow layers of $\sigma_2 \geq 36.97 \text{ kg m}^{-3}$ (ISOW and DSOw, equivalent to $\sigma_\theta \geq 27.80 \text{ kg m}^{-3}$; see Fig. 5), the total westward transport from the northern boundary to about 57.5°N is 9.8 Sv , of which 7.0 Sv is in the narrow boundary current. The tracer transport is $13.3 \times 10^5 \text{ kg s}^{-1}$, of which $8.3 \times 10^5 \text{ kg s}^{-1}$ is in the boundary current. Thus, the interior flows account for slightly less than 30% of the volume transport and 40% of tracer transport, respectively. The DSOw, defined here as $\sigma_2 \geq 37.11 \text{ kg m}^{-3}$ (below the ISOW salinity maximum in Fig. 5), has volume and tracer fluxes of 3.2 Sv and $7.8 \times 10^5 \text{ kg s}^{-1}$; roughly half of these transports (1.8 Sv and $4.4 \times 10^5 \text{ kg s}^{-1}$, respectively) are through the interior flows.

The westward volume and tracer fluxes for all overflow layers below (σ_2) 36.97 kg m^{-3} in E32 (10 Sv and $13.2 \times 10^5 \text{ kg s}^{-1}$, respectively) are similar to those of E64, as are the fluxes for DSOw (3.1 Sv and $6.5 \times 10^5 \text{ kg s}^{-1}$). However, the boundary current is wider in E32, and the separation is less clear between the boundary current and the interior flows because of a recirculation near 60°N (Fig. 9). If we define the interior flow as from the middle of this recirculation to 57.5°N , the interior flow in E32 accounts for about $1/3$ of the volume and tracer fluxes for the DSOw, compared to $1/2$ in E64.

One may wonder about the dynamics responsible for the westward spreading of the deep DSOw from the DWBC into the interior, in particular whether the deep transport deviates significantly from geostrophic current due to Ekman bottom friction (e.g., Price and Baringer 1994). This is difficult to determine in Fig. 7 but becomes clearer when the transport streamfunction ψ is overlaid with the bathymetry (Fig. 10). The results show that the deep flow in the Labrador Sea actually follows the isobaths very closely. Thus, even though the DSOw through the central Labrador Sea appears as an “interior” flow, it would be better described as the broadening of the DWBC over the gentle slope under PV conservation. This dynamical process was first explained by Stommel and Arons (1972), considering the flow of uniform PV entering the DWBC from midocean. In Fig. 11a, we examine the conservation of PV for the model dense DSOw along its streamlines from the Irminger Sea into the Labrador Sea and beyond. The PV is approximately conserved in the transition from a steep bottom slope at the Eirik Ridge to a broad slope in the northern/central Labrador Sea. This process also explains the widespread occurrence of isopycnals lying nearly parallel with the bottom in such DWBCs (Fig. 11b).

The initial descent of the DSOw plume to greater depths takes place in the Irminger Sea, from its initial cascade near the Denmark Strait sill (Girton and Sanford 2003) to farther south around the Eirik Ridge (Fig. 10). It is here that strong entrainment and diapycnal mixing occurs. Subsequently, the overflow plume follows bathymetry until exiting the Labrador Sea and again descending significantly; the velocity core of the DSOw is $\sim 4000 \text{ m}$ at 43°N (Schott et al. 2004, 2006), approximately 1000 m deeper

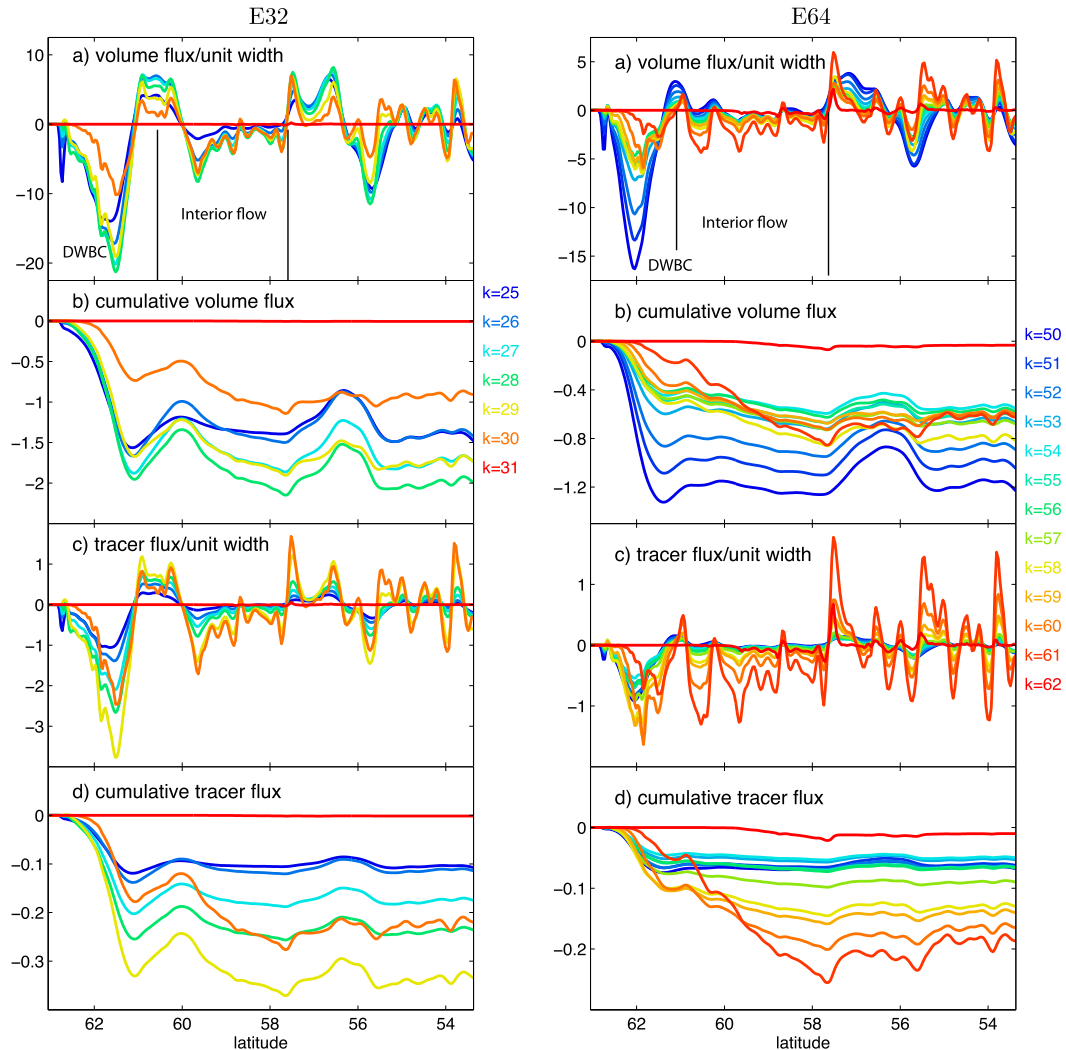


FIG. 9. Modeled layer-by-layer fluxes for all overflow water with $\sigma_2 \geq 36.97 \text{ kg m}^{-3}$, across the central Labrador Sea (red line in Figs. 7–8) in simulations (left) E32 and (right) E64: (a) volume flux per unit width ($\text{m}^2 \text{ s}^{-1}$); (b) southward cumulative volume flux (Sv); (c) tracer flux per unit width ($\text{kg m}^{-1} \text{ s}^{-1}$); and (d) southward cumulative tracer flux (10^6 kg s^{-1}).

than at 53°N (Fischer et al. 2004, 2010). The spreading of DSOW in this region is discussed in the next section.

c. The spreading of DSOW in the Newfoundland basin

After flowing around/across the northern/central Labrador Sea, the DSOW reforms as a narrow DWBC at Hamilton Bank ($\sim 54^\circ\text{N}$) and continues southward along the Labrador coast (Figs. 7–8). In the Newfoundland basin (Fig. 12), the DWBC crosses from subtropical gyre while passing close to the upper limb of the AMOC. This dynamically important region features complex bathymetry around the deep basin and energetic western boundary jets and recirculation cells (in terms of both mean flow and eddy variability).

The southward volume and tracer transports across five sections in the Newfoundland basin are shown in Fig. 13. The net volume transport is $\sim 7 \text{ Sv}$ for the overflow water ($\sigma_2 \geq 36.97 \text{ kg m}^{-3}$) and $\sim 3 \text{ Sv}$ for the DSOW ($\sigma_2 \geq 37.11 \text{ kg m}^{-3}$). The tracer transport gradually decreases from $1.1 \times 10^6 \text{ kg s}^{-1}$ near 53°N to $0.8 \times 10^6 \text{ kg s}^{-1}$ near 43°N , implying an ongoing accumulation of tracer inventory in the Newfoundland basin. The transport structure varies significantly from 53° to 43°N (Fig. 13): (i) Near 53°N the southward transport is completely within the narrow DWBC, with some offshore return flow in the upper overflow layer. (ii) Across the Orphan Knoll section, the upper overflow water flows through the west passage (slightly shallower than 3000 m), whereas most of the DSOW is forced to flow

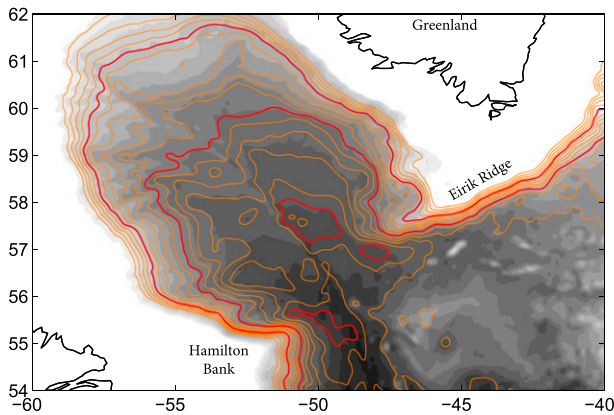


FIG. 10. Streamfunction ψ (lines) of the DSW ($\sigma_2 \geq 37.11$) from simulation E64 overlaid on the bathymetry (gray shading with 100-m interval; area shallower than 2500 m in white). Each ψ contour is 0.2 Sv for orange lines and 1 Sv for red lines.

south through the deep basin east of Orphan Knoll. There is strong eddy activity and recirculation farther offshore. (iii) At 47°N, the transport is southward in the boundary current east of the Flemish Cap, northward offshore, and southward again farther east. Rhein et al. (2011) found a similar flow pattern at 47°N based on repeat LADCP surveys. (iv) At 44°N, there exists a strong cyclonic recirculation cell, and some southward

transport takes place to the east of the Milne Seamounts (MS). (v) Farther south across the section near 43°N, the recirculation is much weaker as compared to the three upstream sections, and the DSW spreads over a wide range, somewhat similar to the central Labrador Sea.

The pattern of tracer transport is quite similar to the volume transport, except that the tracer flux is mostly in the DSW (Fig. 13) due to its injection there. Also, the transport patterns in E32 (not shown) are generally similar to those in E64. In the rest of this subsection we focus on three aspects of the circulation that are key to the DSW spreading in the Newfoundland basin: topography, recirculation, and eddy variability.

1) FLOW SEPARATION AND SINKING DUE TO ABRUPT TOPOGRAPHIC CHANGE

Orphan Knoll near 50.5°N and 46.5°W poses an abrupt topographic change to the DWBC. As shown in Fig. 13b, the upper overflow water is allowed to pass through its west channel. Most of the DSW, however, is forced to flow northeastward before steering southward along a steep “wall” east of Orphan Knoll. In doing so, the DSW is forced to flow across the isobaths and descends into the deep basin. This is illustrated in Fig. 14: upstream of Orphan Knoll, the bottom-trapped DSW flows along the isobath of ~3400 m all the way to about

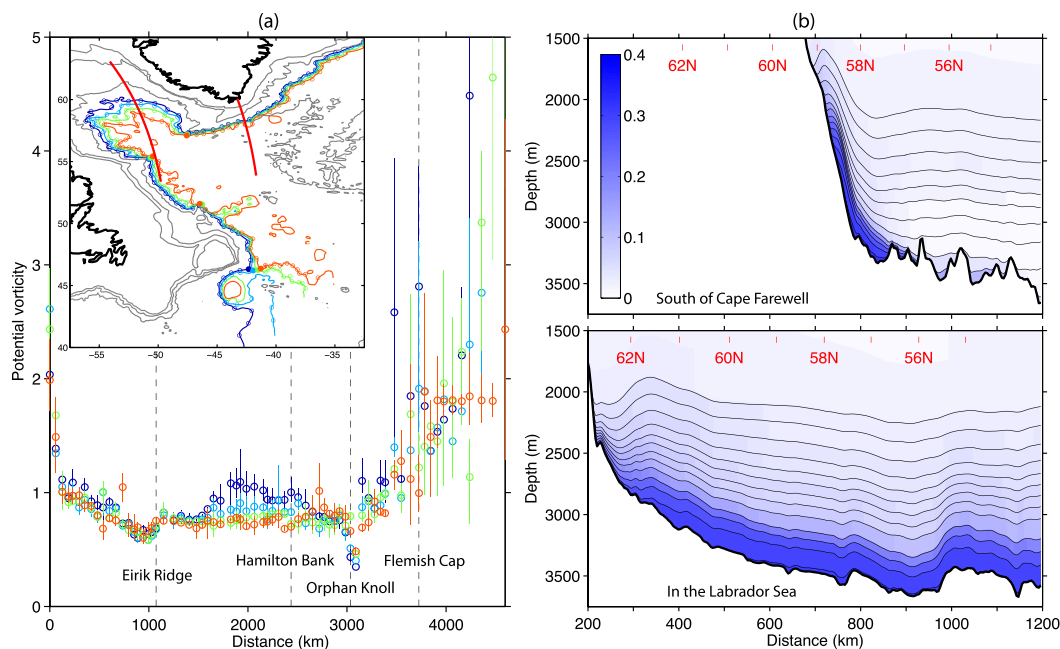


FIG. 11. (a) PV ($10^{-6} \text{ m}^{-1} \text{ s}^{-1}$) of the dense DSW ($\sigma_2 \geq 37.14 \text{ kg m}^{-3}$). Circles and vertical lines are the averages and ranges of PV within 10 km of the selected points along four transport streamlines, denoted as circles along the lines in the inset map. (b) Tracer concentration along two model sections (red lines in the map and in Figs. 7–8) south of Cape Farewell (steep slope) and in the central Labrador Sea (gentle slope). The black lines denote the model layer interfaces for overflow water.

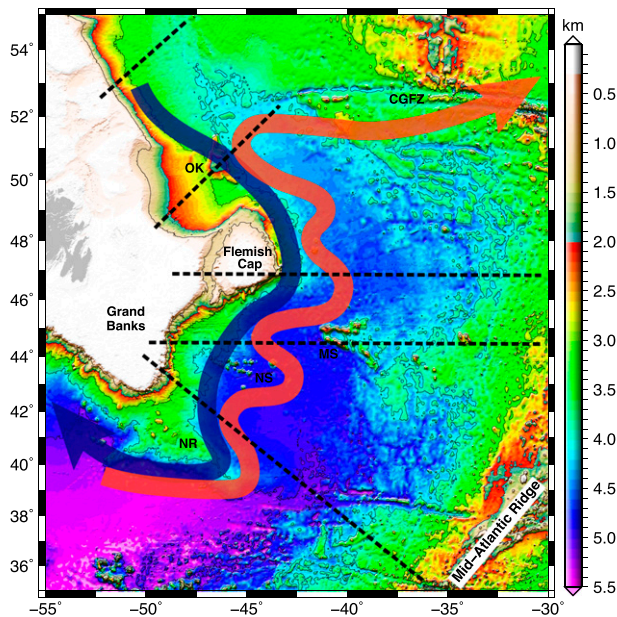


FIG. 12. Bathymetry of the Newfoundland basin along with schematic pathways for (red) the North Atlantic Current (Rossby 1996) and (blue) the deep western boundary current. Key topographic features include NR, NS, MS, OK, and CGFZ. The black dashed lines denote locations of five model sections across which fluxes are examined (Fig. 13).

47°W. After flowing around the northern tip of Orphan Knoll, most of the DSW transport is found deeper than 3800 m. The overall transport-weighted depth for DSW increased ~ 460 m when flowing around this relatively small topographic feature, nearly half of the total depth change observed between 53° and 43°N. Also, as the DSW plume flows around Orphan Knoll and descends into the deep Newfoundland basin, it becomes thicker (probably due to enhanced diapycnal mixing), and the PV is not conserved along the streamline (Fig. 14b). This is quite different from the scenario in the deep Labrador Sea, where the plume generally follows isobaths (Fig. 10) and the PV is roughly conserved (Figs. 7b, 11a).

2) RECIRCULATION IN THE NEWFOUNDLAND BASIN

Figure 14 shows a clear cyclonic recirculation cell offshore of Orphan Knoll, surrounding the area of maximum tracer inventory and a low PV (note how the zonal ridge near 52°N, 46°W corresponds to a small area of low inventory and high PV inside the recirculation). The underlying dynamics for the modeled and observed offshore maximum in tracer inventory can be explained as follows: The recirculation carries tracer from the DWBC of high concentration into the interior where

the corresponding low PV acts like a “container.” It encloses a thick body of water into which the tracer leaks or diffuses (by eddies) as a result of the surrounding recirculation and builds up the inventory until the concentration matches up with the surrounding. Examination of the time series of tracer concentration (not shown) suggests that it takes ~ 10 yr to reach a relatively stable state in this area from the time it is released at the strait. This relatively short time highlights the effectiveness of recirculation in spreading the DSW tracer from the boundary current into the interior when compared to diapycnal and isopycnal mixing time scales.

The recirculation off Orphan Knoll is not unique. Figure 15 displays the transport streamfunction and tracer inventory for the DSW ($\sigma_2 \geq 37.11 \text{ kg m}^{-3}$) on a broader scale. The results, consistent between E32 and E64, show that there exist a series of cyclonic recirculation cells (labeled A–D in Fig. 15), all associated with a relatively high tracer inventory. It is reasonable to ask whether the model recirculation is realistic. This is difficult to know for certain, as long-term current observations are typically made along the boundary and rarely in the recirculation regimes. However, our model results are consistent with the few available observations. Lazier (1994) deployed four moorings in the northwestern corner of the NAC for ~ 250 days (red circles in Fig. 14) and found a strong deep current of $5\text{--}8 \text{ cm s}^{-1}$ at 3500 m at two southern mooring locations. The model northeastward flow of DSW, perpendicular to Orphan Knoll as part of the recirculation cell A, is similar to this observation, except that it is located slightly to the north and is strongest between the two middle mooring locations. To the south, Rhein et al. (2011) observed a similar meridional flow pattern along 47°N as mentioned; the oxygen section in Pickart and Huang (1995) indicates a cyclonic recirculation near 44°N (their Fig. 17). At the southern edge of the Newfoundland Ridge (NR), Armi and Williams (1991) examined θ and velocity data at two deep moorings with very good vertical resolution and found the westward flow of DSW into the recirculation gyre of NADW (see their Fig. 15 and discussion), supporting the model velocity/tracer pattern shown in Fig. 15.

The question then arises as to what drives these deep recirculation cells. For the northeastward flow perpendicular to the DWBC off Orphan Knoll, the observations of Lazier (1994) and the model results suggest that not only are the mean upper and deep currents in the same direction (stronger current in upper layer), but also that the current variability is very similar. This suggests that variability of the strong western boundary current in the upper ocean, that is, the NAC, may be the driving force for the deep recirculation. To explore this

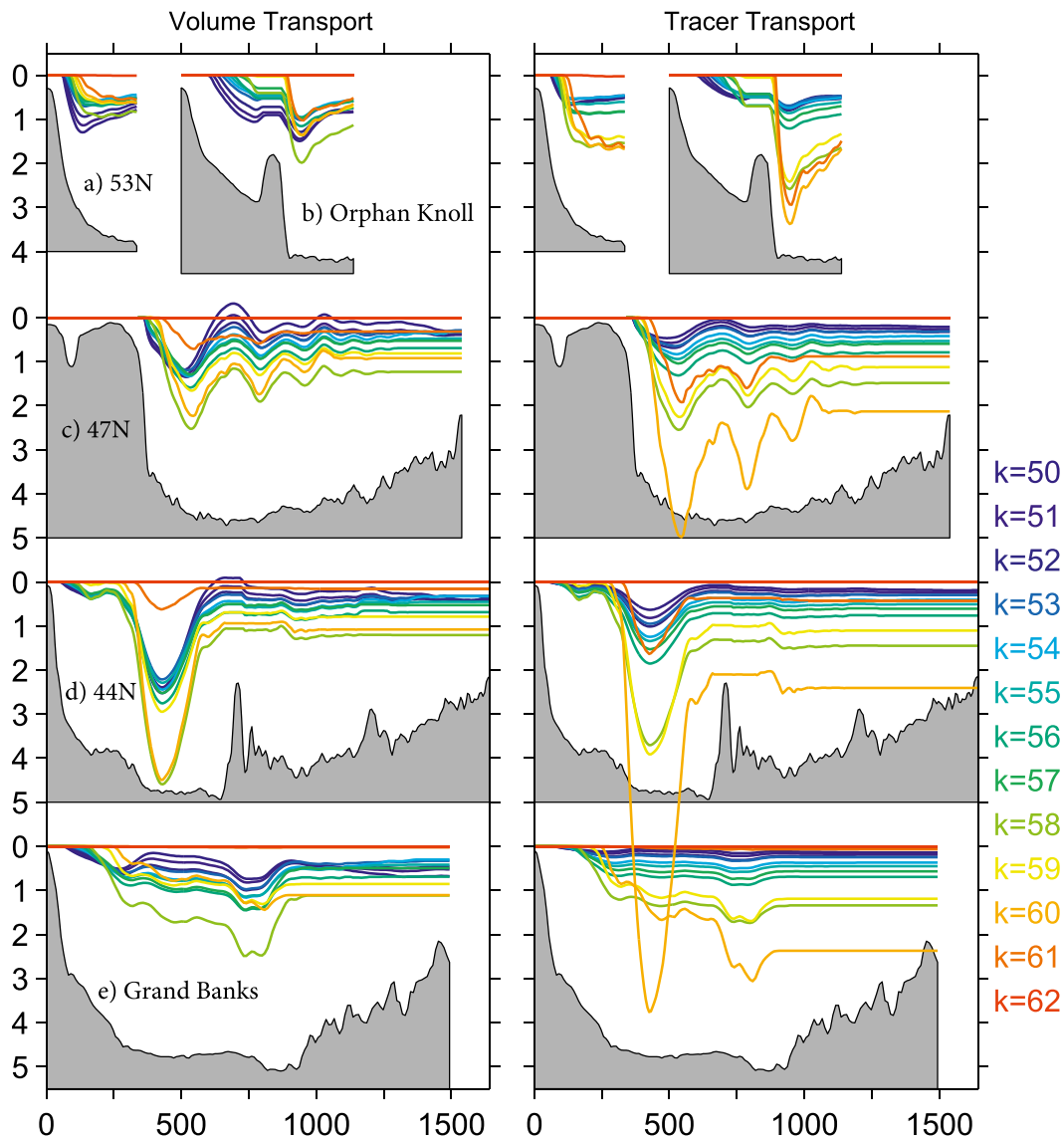


FIG. 13. (left) Time-mean southward volume transport (Sv) and (right) tracer transport (10^5 kg s^{-1}) across five sections in the Newfoundland basin (Fig. 12). The transports are cumulative eastward for each isopycnal layer below 36.97 kg m^{-3} based on E64 (years 16–20). The gray shading denotes the bottom bathymetry in kilometers.

hypothesis further, the circulation pattern for the upper limb of the AMOC ($\sigma_2 \leq 36.70 \text{ kg m}^{-3}$) is shown in Fig. 16. The results indicate that the deep cyclonic cells are located slightly to the north-northwest of the upper anticyclonic recirculation cells, also labeled as A–D in Fig. 16, so the east-northeastward flows are in the same direction. The upper anticyclonic cells associated with the meandering of the NAC have been well documented in Rossby (1996) and can be seen in the time-mean sea surface height data (Rio et al. 2011). The model NAC pathway agrees with the schematics of Rossby (1996), including the location of anticyclonic cells. One key issue in Fig. 16 is that, in the model, the Mann eddy (cell

D) is weaker than the cell C near 47°N , whereas, in observations, the semipermanent Mann eddy is clearly the stronger one.

Thus, we believe that the meandering of the upper NAC is the primary driving mechanism for the deep recirculation gyres. Note how the stronger circulation around deep cells A–C in E32 (Fig. 15) corresponds to a stronger upper NAC and anticyclonic cells (Fig. 16). A plausible explanation is that after encountering the deep circulation laterally at $40^\circ\text{--}45^\circ\text{N}$, where strong mixing occurs between NAC water and the LSW lying west of it, the NAC interacts vertically, through eddy form stress, and drags the DSOW offshore. Interfacial form stress,

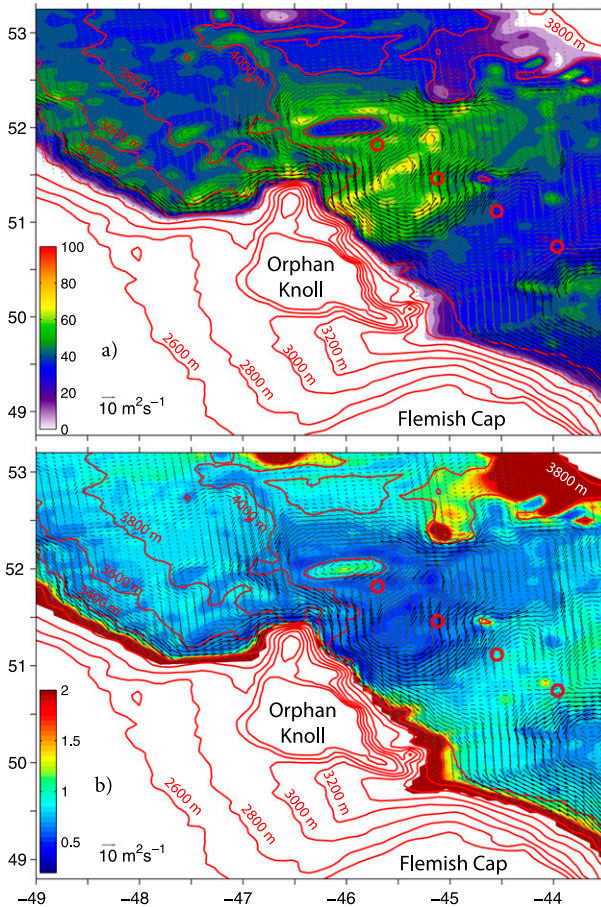


FIG. 14. Mean deep circulation around Orphan Knoll for $\sigma_2 \geq 37.14 \text{ kg m}^{-3}$ based on simulation E64 (years 16–20). Color shading denotes (a) tracer inventory (kg m^{-2}) and (b) potential vorticity ($10^{-6} \text{ m}^{-1} \text{ s}^{-1}$). Vectors in both panels are transport per unit width; values higher than $10 \text{ m}^2 \text{ s}^{-1}$ are denoted in black vectors with a constant length. Red circles are the four mooring locations of Lazier (1994).

like bottom topographic form stress, is the basic pressure drag mechanism that causes the vertical flux of horizontal momentum in much of the ocean and atmosphere (e.g., Rhines and Holland 1979).

The partially enclosed topography of the Newfoundland basin is also an important source of deep recirculation gyres. Pickart and Huang (1995) demonstrated, using an idealized model, how a topographic ridge (like the Newfoundland Ridge) can partially block the DWBC and give rise to cyclonic recirculation of the deepest water. These topographic blocking dynamics, associated with the Newfoundland Seamounts (NS), may have enhanced the model deep recirculation D in Fig. 15 south of the Flemish Cap. Topography around Orphan Knoll may also play a role in the deep recirculation under the northwestern corner of the NAC.

3) EDDY VARIABILITY CONTRIBUTION TO THE TRACER FLUX

Given the high eddy kinetic energy in the Newfoundland basin, it is important to determine to what extent the eddy variability contributes to the tracer flux. The eddy flux can be defined as $[V'C']$, in which the bracket and the primes denote a 5-yr mean and temporal variability relative to the mean values, respectively. Here, V is the layer volume flux (horizontal velocity u times layer thickness h). The temporal mean $[V] = [h][u] + [h'u']$ thus includes eddy bolus transport due to correlated eddy thickness and eddy velocity. This division into mean and eddy layer tracer flux is different from the usual Eulerian form in which the average of the layer-integrated flux $[huC]$ has five terms when expanded into eddy and mean components; here, the eddy flux $[h'V']$ sums up three of those terms.

The eddy flux $[V'C']$ in the western Newfoundland basin around the Flemish Cap is shown in Fig. 17. Compared to the mean flow contribution $[V][C]$, the eddy flux is small in magnitude but exhibits a similar direction that is perpendicular to the DWBC and pointing toward offshore. This flux can be viewed as a horizontal diffusion process, in which the tracers are diffused/mixed from the DWBC (high tracer concentration) toward the deep offshore basin (low concentration) due to eddy motion. We calculated the fluxes across an offshore section that runs roughly parallel to the DWBC (green line in Fig. 17) and compared them to sections running across the DWBC near 53° (red) and 44°N (blue). The results are shown in Fig. 18 for both the E32 and E64. Figure 18 shows that tracer flux across the 53° and 44°N sections is primarily due to the mean flow. Across the offshore section, however, both mean flow and eddy variability contribute to the tracer flux. The eddy contribution is primarily in the DSOW, and the mean flow contribution is primarily in the upper overflow. Figure 18 also shows that the fluxes are generally consistent between the two simulations except that, in E32, the 53°N section captured all the southward fluxes, whereas, in E64, part of these fluxes are through the offshore section.

The fluxes for all the overflow layers ($\sigma_2 \geq 36.97 \text{ kg m}^{-3}$) are summarized in Table 2. In both simulations, approximately 30% of the total southward flux that enters the enclosed area from the north section leaves the boundary current into the interior across the offshore section, and approximately $\frac{2}{3}$ of this offshore flux is due to eddy variability. Thus, the eddy variability around the Flemish Cap carries $\sim 20\%$ of the southward tracer flux from the boundary current into the offshore interior. The mean flow carries only about 10% of the

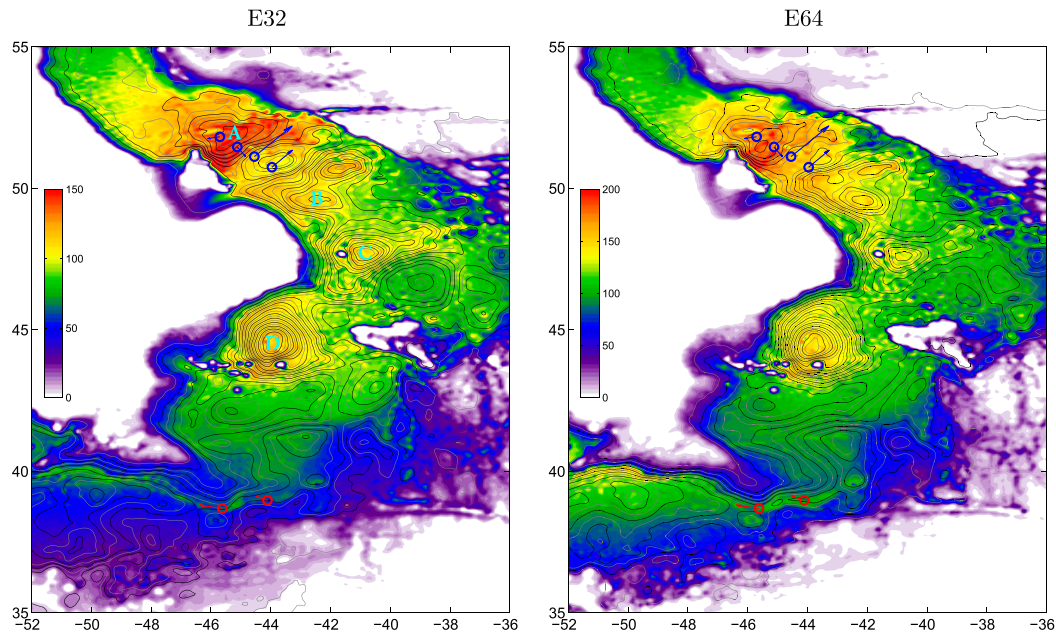


FIG. 15. Streamfunction (contours) over tracer inventory (color shading) for the model DSOW below $\sigma_2 = 37.11 \text{ kg m}^{-3}$ in the Newfoundland basin. The gray/black streamlines have a contour interval of 0.5 Sv. Blue and red vectors are the observed mean deep currents discussed in Lazier (1994) and in Armi and Williams (1991), respectively. Labels A–D marks four cyclonic recirculation cells.

tracer flux but nearly 37% of the volume transport from the boundary current into the offshore interior, mostly in the upper overflow layer (green circled lines in Fig. 18). Roughly half of this offshore volume transport

returns to the north (see Fig. 8); the remainder flows southward east of the Milne Seamounts (see Fig. 13d) as the interior export of overflow water, a topic Lozier et al. (2013) considered in a Lagrangian perspective.

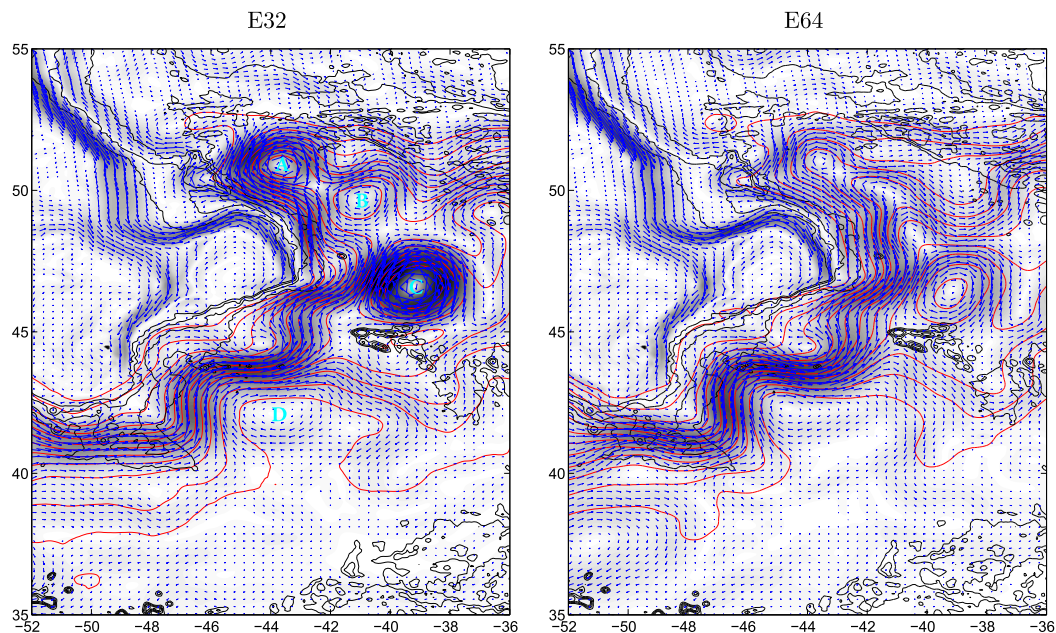


FIG. 16. Modeled mean circulation pattern for the upper limb of the AMOC ($\sigma_2 < 36.70 \text{ kg m}^{-3}$) in the Newfoundland basin. The red contours are the depth of the isopycnal 36.70, increasing from 500 to 1050 m toward offshore. The blue vectors are the vertically averaged velocity (color shading denotes magnitude). Labels A–D marks four anticyclonic recirculation cells.

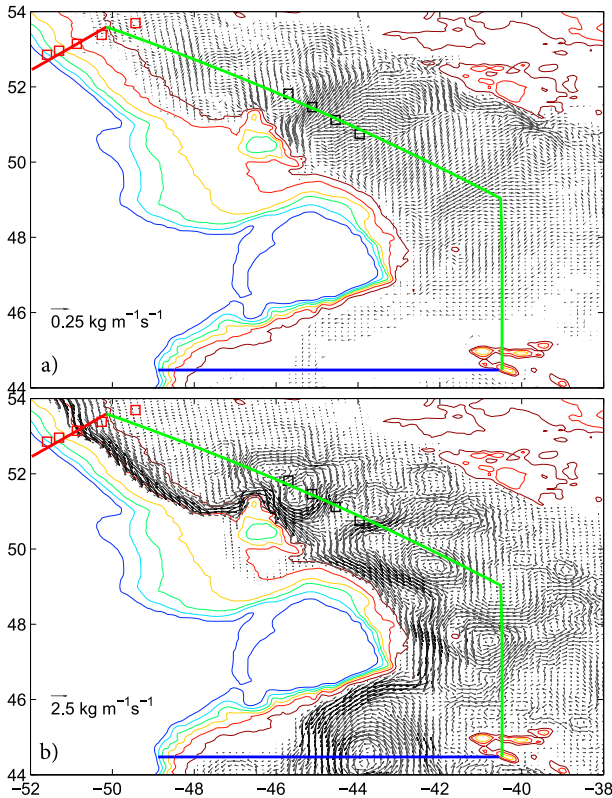


FIG. 17. Model layered tracer fluxes per unit width in the Newfoundland basin around the Flemish Cap: (a) eddy contribution $[V'C]$ and (b) mean flow contribution $[V][C]$. Results are based on a 5-yr mean (years 16–20) in the E64 for isopycnal layer (σ_2) 37.12 kg m^{-3} .

4. Summary and discussion

As a key constituent of North Atlantic Deep Water (NADW), the Denmark Strait overflow water (DSOW) directly impacts water properties and circulation in much of the deep Atlantic Ocean. Complex bottom topography both guides its pathway and stimulates transitions: diapycnal mixing and deepening. Some prominent “fingerlike” ridges are actually sedimentary accumulations shaped by the DWBC and continuing to evolve over time, most notably the Eirik Ridge south of Greenland, the Bjorn and Garder Drifts in the Iceland basin, and the Blake–Bahama Outer Ridge in the western North Atlantic. It is essential to develop accurate high-resolution models of the circulation and downstream evolution of deep water masses through interactions with bottom topographic features. Yet these will always require observational support to locate diapycnal mixing. Fortunately, direct and inferred observations of deep mixing are now more prevalent, following the initial observations of topographic/tidal deep mixing (e.g., Polzin et al. 1997).

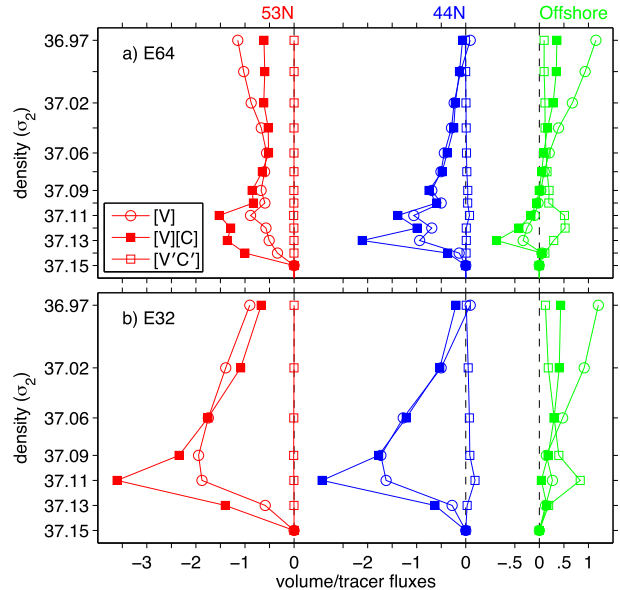


FIG. 18. Model layered volume flux $[V]$ (circles), tracer flux due to mean flow $[V][C]$ (filled squares), and tracer flux due to eddy variability $[V'C]$ (open squares) across three sections as shown in Fig. 17: near 53°N (red), near 44°N (blue), and offshore (green). The units are Sv for volume flux and 10^5 kg s^{-1} for the tracer fluxes. Results are based on a 5-yr mean (years 16–20).

The general flow pattern of the DSOW in the North Atlantic has been depicted effectively using distributions of θ , S , and tracers (CFCs, oxygen, ^{129}I , tritium, etc.). The observed DSOW exhibits shared transport between narrow deep boundary currents and interior pathways as seen in many parts of the World Ocean. In this study, we used numerical results from eddy-resolving simulations to study the mechanisms

TABLE 2. The budget of tracer fluxes and volume transports for the overflow water in the enclosed area in Fig. 14. The results are based on a 5-yr mean (years 16–20) for both 32- and 64-layer simulations. The overflow water is defined as model layers of density σ_2 no less than 36.97 kg m^{-3} (see Table 1). Note that there is a small residual for tracer flux, corresponding to an increase of the tracer inventory.

	E32	E64
Tracer Flux (10^5 kg s^{-1})		
Southward across the northern section	10.9	12.1
Eastward across the offshore section	3.5	3.9
due to eddy variability	2.1	2.6
due to time-mean flow	1.4	1.3
Southward across section near 44°N	6.9	7.5
Residual	0.5	0.7
Volume transport (Sv)		
Southward across the northern section	8.5	9.1
Eastward across the offshore section	3.1	3.5
Southward across section near 44°N	5.4	5.6

controlling this division, which involves both gradual and abrupt variations in bottom topography, and stirring by strong, variable currents overhead.

The model results, generally consistent between two simulations of different vertical resolutions, yielded volume transport as well as θ/S and tracer properties of the DSOE similar to observations in the western subpolar North Atlantic. In particular, the model DSOE showed an increased tracer concentration toward the bottom in the Irminger and Labrador Seas, consistent with the observed ^{129}I and CFC profiles in Smith et al. (2005) and many other studies. Horizontally, model tracer inventory was nearly homogenous across the central Labrador Sea and exhibited a local maximum in the area near Orphan Knoll and the Flemish Cap, qualitatively in good agreement with the observed CFC distribution (LeBel et al. 2008).

A number of dynamical processes are involved in the spreading of overflow water: 1) the Ekman layer near the bottom and entrainment mixing across the upper interface; 2) gradual topographic change or the broadening of DWBC over gentle slopes with conserved PV; 3) abrupt topographic change that results in flow steering/separation, in which PV is not conserved; and 4) recirculation into the deep basin forced by the meandering upper-ocean western boundary current and/or by topographic effects.

In the Irminger Sea, the DSOE plume descends/spreads across the isobaths primarily due to the frictional Ekman layer at the bottom and the diapycnal mixing across the upper overflow interface, resulting in a secondary circulation perpendicular to its primary flow pathway (e.g., Price and Baringer 1994). In the northern and central Labrador Sea, the DSOE transits from a narrow DWBC into a widely spread westward interior flow due to the broadening of the DWBC over a gentle slope under PV conservation (Stommel and Arons 1972). The flow pattern provided a simple, yet plausible, explanation for the observed DSOE tracer distribution across the deep Labrador Sea. Some of the model westward flows turned southeastward along the northwest Atlantic midocean channel in the central Labrador Sea, consistent with the results based on the repeat LADCP surveys along the hydrographic section AR7W (Hall et al. 2013).

Farther downstream into the Newfoundland basin, the circulation is more complex and involves multiple dynamics/processes. First, abrupt topographic change at Orphan Knoll forces the DSOE to flow and descend into the deep basin to the east of Orphan Knoll. Second, the DSOE flows into a series of cyclonic recirculation cells in the deep Newfoundland basin. The recirculation cell offshore of Orphan Knoll–Flemish Cap is the mechanism behind the localized maximum for the CFC

inventories observed in LeBel et al. (2008). These cyclonic cells in the deep are collocated with anticyclonic cells in the upper layer, and we believe the meandering of the strong North Atlantic Current is the primary driving mechanism for the cyclonic deep recirculation. Other mechanisms, such as topographic blocking (of the Newfoundland seamounts), may play additional roles in the strong cyclonic recirculation near 44°N , south of the Flemish Cap.

Eddy variability also contributes a tracer flux from the DWBC into the offshore interior without a mean volume/mass flux. This can be clearly seen in the area around the Flemish Cap, where the eddy flux is in a similar direction, perpendicular to the DWBC toward offshore (Fig. 17), and comparable to the downgradient, horizontal diffusion process. Integration along a section roughly parallel to the DWBC suggests that the eddy fluxes carry about 20% of the tracer transport in the DWBC into the offshore interior. This flux contributes to the tracer inventory maximum that is found in both observations and models in the deep basin offshore of the DWBC.

Acknowledgments. This work is supported by ONR Award N00014-09-1-0587, the NSF Physical Oceanography Program, and NASA Ocean Surface Topography Science Team Program. We wish to thank William Smethie (Lamont-Doherty Earth Observatory) and Elsevier for permission to include Fig. 1, John Smith (Fisheries and Oceans Canada) who kindly provided the ^{129}I profiles used in Fig. 6, and Alan Wallcraft (NRL/SSC) for tremendous help on tracer scheme in HYCOM. The numerical simulations were performed on supercomputers at the Navy Department of Defense (DoD) Supercomputing Resource Center (DSRC), Stennis Space Center, Mississippi, using computer time provided by the U.S. DoD High Performance Computing Modernization Program.

REFERENCES

- Armi, L., and R. Williams, 1991: The deep western boundary undercurrent off the Newfoundland Ridge. *Deep-Sea Res.*, **38**, 371–391, doi:10.1016/0198-0149(91)90074-P.
- Bacon, S., and P. M. Saunders, 2010: The deep western boundary current at Cape Farewell: Results from a moored current meter array. *J. Phys. Oceanogr.*, **40**, 815–829, doi:10.1175/2009JPO4091.1.
- Biastoch, A., C. W. Böning, J. Getzlaff, J.-M. Molines, and G. Madec, 2008: Causes of interannual–decadal variability in the meridional overturning circulation of the midlatitude North Atlantic Ocean. *J. Climate*, **21**, 6599–6615, doi:10.1175/2008JCL2404.1.
- Bleck, R., 2002: An oceanic general circulation model framed in hybrid isopycnic–Cartesian coordinates. *Ocean Modell.*, **4**, 55–88, doi:10.1016/S1463-5003(01)00012-9.

- Böning, C. W., M. Scheinert, J. Dengg, A. Biastoch, and A. Funk, 2006: Decadal variability of subpolar gyre transport and its reverberation in the North Atlantic overturning. *Geophys. Res. Lett.*, **33**, L21S01, doi:10.1029/2006GL026906.
- Bower, A. S., M. S. Lozier, S. F. Gary, and C. W. Böning, 2009: Interior pathways of the North Atlantic meridional overturning circulation. *Nature*, **459**, 243–247, doi:10.1038/nature07979.
- , —, and —, 2011: Export of Labrador Sea Water from the subpolar North Atlantic: A Lagrangian perspective. *Deep-Sea Res. II*, **58**, 1798–1818, doi:10.1016/j.dsr2.2010.10.060.
- Bryden, H. L., W. E. Johns, and P. M. Saunders, 2005: Deep western boundary current east of Abaco: Mean structure and transport. *J. Mar. Res.*, **63**, 35–57, doi:10.1357/0022240053693806.
- Carnes, M. R., 2009: Description and evaluation of GDEM-V 3.0. Naval Research Laboratory Tech. Rep. NRL/MR/7330-09-9165, 21 pp. [Available online at <http://www7320.nrlssc.navy.mil/pubs/2009/carnes-2009.pdf>.]
- Chassignet, E. P., L. T. Smith, G. R. Halliwell, and R. Bleck, 2003: North Atlantic simulations with the Hybrid Coordinate Ocean Model (HYCOM): Impact of the vertical coordinate choice, reference pressure, and thermobaricity. *J. Phys. Oceanogr.*, **33**, 2504–2526, doi:10.1175/1520-0485(2003)033<2504:NASWTH>2.0.CO;2.
- Clarke, R. A., H. W. Hill, R. F. Reiniger, and B. A. Warren, 1980: Current system south and east of the Grand Banks of Newfoundland. *J. Phys. Oceanogr.*, **10**, 25–65, doi:10.1175/1520-0485(1980)010<0025:CSSAEO>2.0.CO;2.
- , R. M. Hendry, and I. Yashayaev, 1998: A western boundary current meter array in the North Atlantic near 42°N. *International WOCE Newsletter*, No. 33, WOCE International Project Office, Southampton, United Kingdom, 33–34. [Available online at <http://www.nodc.noaa.gov/woce/wdiu/wocedocs/newsltr/news33/news33.pdf>.]
- Dickson, R. R., and J. Brown, 1994: The production of North Atlantic Deep Water: Source, rates, and pathways. *J. Geophys. Res.*, **99**, 12 319–12 341, doi:10.1029/94JC00530.
- , I. Yashayaev, J. Meincke, B. Turrell, S. Dye, and J. Holfort, 2002: Rapid freshening of the deep North Atlantic over the past four decades. *Nature*, **416**, 832–837, doi:10.1038/416832a.
- , and Coauthors, 2008: The overflow flux west of Iceland: Variability, origins, and forcing. *Arctic-Subarctic Ocean Fluxes: Defining the Role of the Northern Seas in Climate*, R. R. Dickson, J. Meincke, and P. B. Rhines, Eds., Springer, 443–474, doi:10.1007/978-1-4020-6774-7_20.
- Fischer, J., F. A. Schott, and M. Dengler, 2004: Boundary circulation at the exit of the Labrador Sea. *J. Phys. Oceanogr.*, **34**, 1548–1570, doi:10.1175/1520-0485(2004)034<1548:BCATEO>2.0.CO;2.
- , M. Visbeck, R. Zantopp, and N. Nunes, 2010: Interannual to decadal variability of outflow from the Labrador Sea. *Geophys. Res. Lett.*, **37**, L24610, doi:10.1029/2010GL045321.
- Gary, S. F., M. Susan Lozier, C. W. Böning, and A. Biastoch, 2011: Deciphering the pathways for the deep limb of the meridional overturning circulation. *Deep-Sea Res. II*, **58**, 1781–1797, doi:10.1016/j.dsr2.2010.10.059.
- Girton, J. B., and T. B. Sanford, 2003: Descent and modification of the overflow plume in the Denmark Strait. *J. Phys. Oceanogr.*, **33**, 1351–1363, doi:10.1175/1520-0485(2003)033<1351:DAMOTO>2.0.CO;2.
- Hall, M. M., D. J. Torres, and I. Yashayaev, 2013: Absolute velocity along the AR7W section in the Labrador Sea. *Deep-Sea Res. I*, **72**, 72–87, doi:10.1016/j.dsr.2012.11.005.
- Holland, W. R., and P. B. Rhines, 1980: An example of eddy-induced ocean circulation. *J. Phys. Oceanogr.*, **10**, 1010–1031, doi:10.1175/1520-0485(1980)010<1010:AEOEIO>2.0.CO;2.
- Jenkins, W. J., and P. B. Rhines, 1980: Tritium in the deep North Atlantic Ocean. *Nature*, **286**, 877–880, doi:10.1038/286877a0.
- Jochumsen, K., D. Quadfasel, H. Valdimarsson, and S. Jónsson, 2012: Variability of the Denmark Strait overflow: Moored time series from 1996–2011. *J. Geophys. Res.*, **117**, C12003, doi:10.1029/2012JC008244.
- Johns, W. E., L. M. Beal, M. O. Baringer, J. R. Molina, S. A. Cunningham, T. Kanzow, and D. Rayner, 2008: Variability of shallow and deep western boundary currents off the Bahamas during 2004–05: Results from the 26°N RAPID–MOC array. *J. Phys. Oceanogr.*, **38**, 605–623, doi:10.1175/2007JPO3791.1.
- Kanzow, T., and W. Zenk, 2014: Structure and transport of the Iceland Scotland Overflow plume along the Reykjanes Ridge in the Iceland basin. *Deep-Sea Res. I*, **86**, 82–93, doi:10.1016/j.dsr.2013.11.003.
- Klaucke, I., and R. Hesse, 1996: Fluvial features in the deep-sea: New insights from the glacialic submarine drainage system of the Northwest Atlantic Mid-Ocean Channel in the Labrador Sea. *Sediment. Geol.*, **106**, 223–234, doi:10.1016/S0037-0738(96)00008-5.
- Large, W. G., J. C. McWilliams, and S. C. Doney, 1994: Ocean vertical mixing: A review and a model with a nonlocal boundary layer parameterization. *Rev. Geophys.*, **32**, 363–403, doi:10.1029/94RG01872.
- Lazier, J. R. N., 1994: Observations in the northwest corner of the North Atlantic Current. *J. Phys. Oceanogr.*, **24**, 1449–1463, doi:10.1175/1520-0485(1994)024<1449:OITNCO>2.0.CO;2.
- , R. Hendry, A. Clarke, I. Yashayaev, and P. Rhines, 2002: Convection and restratification in the Labrador Sea, 1990–2000. *Deep-Sea Res. I*, **49**, 1819–1835, doi:10.1016/S0967-0637(02)00064-X.
- LeBel, D. A., and Coauthors, 2008: The formation rate of North Atlantic Deep Water and Eighteen Degree Water calculated from CFC-11 inventories observed during WOCE. *Deep-Sea Res. I*, **55**, 891–910, doi:10.1016/j.dsr.2008.03.009.
- Lozier, M. S., S. F. Gary, and A. S. Bower, 2013: Simulated pathways of the overflow waters in the North Atlantic: Subpolar to subtropical export. *Deep-Sea Res. II*, **85**, 147–153, doi:10.1016/j.dsr2.2012.07.037.
- Mauritzen, C., 1996: Production of dense overflow waters feeding the North Atlantic across the Greenland-Scotland Ridge. Part 1: Evidence for a revised circulation scheme. *Deep-Sea Res. I*, **43**, 769–806, doi:10.1016/0967-0637(96)00037-4.
- Orre, S., J. N. Smith, V. Alfimov, and M. Bentsen, 2009: Simulating transport of ¹²⁹I and idealized tracers in the North Atlantic Ocean. *Environ. Fluid Mech.*, **10**, 213–233, doi:10.1007/s10652-009-9138-3.
- Pickart, R. S., and R. X. Huang, 1995: Structure of an inertial deep western boundary current. *J. Mar. Res.*, **53**, 739–770, doi:10.1357/0022240953213007.
- , D. J. Torres, and R. A. Clarke, 2002: Hydrography of the Labrador Sea during active convection. *J. Phys. Oceanogr.*, **32**, 428–457, doi:10.1175/1520-0485(2002)032<0428:HOTLSD>2.0.CO;2.
- Polzin, K. L., J. M. Toole, J. R. Ledwell, and R. W. Schmitt, 1997: Spatial variation of turbulent mixing in the abyssal ocean. *Science*, **276**, 93–96, doi:10.1126/science.276.5309.93.

- Price, J. F., and M. O. Baringer, 1994: Outflows and deep water production by marginal seas. *Prog. Oceanogr.*, **33**, 161–200, doi:10.1016/0079-6611(94)90027-2.
- Rhein, M., and Coauthors, 2002: Labrador Sea Water: Pathways, CFC inventory, and formation rates. *J. Phys. Oceanogr.*, **32**, 648–665, doi:10.1175/1520-0485(2002)032<0648:LSWPCI>2.0.CO;2.
- , D. Kieke, S. H. Kabus, A. Roessler, C. Mertens, R. Meissner, C. W. Böning, and I. Yashayaev, 2011: Deep water formation, the subpolar gyre, and the meridional overturning circulation in the subpolar North Atlantic. *Deep-Sea Res. II*, **58**, 1819–1832, doi:10.1016/j.dsr2.2010.10.061.
- Rhines, P. B., and W. R. Holland, 1979: A theoretical discussion of eddy-driven mean flows. *Dyn. Atmos. Oceans*, **3**, 289–325, doi:10.1016/0377-0265(79)90015-0.
- Rio, M. H., S. Guinehut, and G. Larnicol, 2011: New CNES-CLS09 global mean dynamic topography computed from the combination of GRACE data, altimetry, and in situ measurements. *J. Geophys. Res.*, **116**, C07018, doi:10.1029/2010JC006505.
- Rosmond, T., J. Teixeira, M. Peng, T. Hogan, and R. Pauley, 2002: Navy Operational Global Atmospheric Prediction System (NOGAPS): Forcing for ocean models. *Oceanography*, **15**, 99–108, doi:10.5670/oceanog.2002.40.
- Ross, C. K., 1984: Temperature-salinity characteristics of the ‘overflow’ water in Denmark Strait during OVERFLOW ‘73’. *Rapp. P. V. Reun. Cons. Int. Explor. Mer*, **185**, 111–119.
- Rosby, T., 1996: The North Atlantic Current and surrounding waters: At the crossroads. *Rev. Geophys.*, **34**, 463–481, doi:10.1029/96RG02214.
- Schott, F. A., L. Stramma, R. Zantopp, M. Dengler, J. Fischer, and M. Wibaux, 2004: Circulation and deep water export at the western exit of the subpolar North Atlantic. *J. Phys. Oceanogr.*, **34**, 817–843, doi:10.1175/1520-0485(2004)034<0817:CADEAT>2.0.CO;2.
- , J. Fischer, M. Dengler, and R. Zantopp, 2006: Variability of the deep western boundary current east of the Grand Banks. *Geophys. Res. Lett.*, **33**, L21S07, doi:10.1029/2006GL026563.
- Smethie, W. M., Jr., and R. A. Fine, 2001: Rates of North Atlantic Deep Water formation calculated from chlorofluorocarbon inventories. *Deep-Sea Res. I*, **48**, 189–215, doi:10.1016/S0967-0637(00)00048-0.
- , —, A. Putzka, and E. P. Jones, 2000: Tracing the flow of North Atlantic Deep Water using chlorofluorocarbons. *J. Geophys. Res.*, **105**, 14 297–14 323, doi:10.1029/1999JC900274.
- Smith, J. N., E. P. Jones, S. B. Moran, W. M. Smethie Jr., and W. E. Kieser, 2005: Iodine 129/CFC 11 transit times for Denmark Strait overflow water in the Labrador and Irminger Seas. *J. Geophys. Res.*, **110**, C05006, doi:10.1029/2004JC002516.
- Stommel, H., and A. B. Arons, 1972: On the abyssal circulation of the World Ocean—V. The influence of bottom slope on the broadening of inertial boundary currents. *Deep-Sea Res. Oceanogr. Abstr.*, **19**, 707–718, doi:10.1016/0011-7471(72)90062-9.
- Toole, J. M., R. G. Curry, T. M. Joyce, M. McCartney, and B. Peña-Molino, 2011: Transport of the North Atlantic deep western boundary current about 39°N, 70°W: 2004–2008. *Deep-Sea Res. II*, **58**, 1768–1780, doi:10.1016/j.dsr2.2010.10.058.
- Uppala, S. M., and Coauthors, 2005: The ERA-40 Re-Analysis. *Quart. J. Roy. Meteor. Soc.*, **131**, 2961–3012, doi:10.1256/qj.04.176.
- Worthington, L. V., and W. R. Wright, 1970: *North Atlantic Ocean Atlas of Potential Temperature and Salinity in the Deep Water including Temperature, Salinity and Oxygen Profiles from the Erika Dan Cruise of 1962*. Vol. 2. Woods Hole Oceanographic Institution, 24 pp.
- Xu, X., W. J. Schmitz Jr., H. E. Hurlburt, P. J. Hogan, and E. P. Chassignet, 2010: Transport of Nordic Seas overflow water into and within the Irminger Sea: An eddy-resolving simulation and observations. *J. Geophys. Res.*, **115**, C12048, doi:10.1029/2010JC006351.
- , —, —, and —, 2012: Mean Atlantic meridional overturning circulation across 26.5°N from eddy-resolving simulations compared to observations. *J. Geophys. Res.*, **117**, C03042, doi:10.1029/2011JC007586.
- , H. E. Hurlburt, W. J. Schmitz Jr., R. J. Zantopp, J. Fischer, and P. J. Hogan, 2013: On the currents and transports connected with the Atlantic meridional overturning circulation in the subpolar North Atlantic. *J. Geophys. Res. Oceans*, **118**, 502–516, doi:10.1002/jgrc.20065.
- , E. P. Chassignet, W. E. Johns, W. J. Schmitz Jr., and E. J. Metzger, 2014: Intraseasonal to interannual variability of the Atlantic meridional overturning circulation from eddy-resolving simulations and observations. *J. Geophys. Res. Oceans*, **119**, 5140–5159, doi:10.1002/2014JC009994.
- Yashayaev, I., 2007: Hydrographic changes in the Labrador Sea, 1960–2005. *Prog. Oceanogr.*, **73**, 242–276, doi:10.1016/j.pocean.2007.04.015.
- , and R. R. Dickson, 2008: Transformation and fate of overflow in the northern North Atlantic. *Arctic-Subarctic Ocean Fluxes: Defining the Role of the Northern Seas in Climate*, R. R. Dickson, J. Meincke, and P. B. Rhines, Eds., Springer, 505–526.
- , M. Bersch, and H. M. van Aken, 2007: Spreading of the Labrador Sea Water to the Irminger and Iceland basins. *Geophys. Res. Lett.*, **34**, L10602, doi:10.1029/2006GL028999.